# Precoding for MIMO Uplink Transmission Over EM-Lens-Based Correlated Channels

George Yammine, Sebastian Stern and Robert F.H. Fischer
Institut für Nachrichtentechnik, Universität Ulm, Ulm, Germany
Email: {george.yammine, sebastian.stern, robert.fischer}@uni-ulm.de

***Abstract*—In multiple-input/multiple-output (MIMO) systems, advanced equalization or precoding schemes are not only known for providing interference mitigation, but they also have been proven to exploit the MIMO channel's diversity. However, in the case of massive MIMO, the computational complexity of such schemes make them unfeasible. To solve this problem for the uplink scenario, an electromagnetic (EM) lens may be employed at the receiver. It effectively focuses the received power onto a smaller number of antennas. Hence, the application of techniques known from classical (non-massive) MIMO systems is enabled in MIMO systems with a large number of antennas. However, building such EM-lens-enabled systems comes with a drawback. Due to physical limitations, it may be impossible to space the antenna elements in a way to provide spatially decoupled channels at the receiver, which results in a performance loss. In this paper, this issue is addressed by first extending the EM-lens-enabled system to include multiple antennas at the transmitter. Following this, different equalization strategies for this scenario are assessed. The performance of the proposed strategies is evaluated by means of numerical simulations. To this end, different levels of spatial channel correlations are considered for both uncoded and coded transmission.**

## I. Introduction

With increasing demand for spectral and power efficiency in non-cooperative multi-user multiple-input/multiple-output (MIMO) systems, *massive MIMO* systems—where a few users communicate with a central base station equipped with a very large number of antennas—, gain more and more attention, e.g., in [9], [11]. However, disadvantages of such systems include the computational requirements for signal processing, and the physical dimensions required to construct such receiver arrays.

In order to reduce the operational overhead, systems that are equipped with an *electromagnetic lens* (EM lens) have been proposed in [20]. For each user/transmitter (equipped with one single antenna), the lens focuses the related received power onto a (small) subset of antennas at the base station. This smaller footprint reduces the required computational cost for signal processing and hence enables techniques that are well suited for classical MIMO (where the number of transmit and receive antennas are of the same small order).

However, when constructing such EM-lens-enabled systems, size restrictions are imposed. That can lead to an inter-antenna spacing at the receiver such that, as a consequence, correlated channels may be present. This in turn reduces the effective dimensionality (degrees of freedom) of the system, resulting in a performance degradation [17]. To deal with this degradation, suited detection schemes must be employed.

This work was supported by Deutsche Forschungsgemeinschaft (DFG) under grant FI 982/12-1.

In this paper, we present an extension to the EM-lens-enabled uplink system, where the users are equipped with multiple transmit antennas. We then analyze the performance of different strategies that are applicable to the scenario in hand. This includes the transmission via singular value decomposition (SVD) which is well-known from classical (non-massive) point-to-point MIMO [16]. Besides, the philosophy of lattice-reduction-aided linear equalization (LRA LE) [19], [18] is adapted to the scenario in hand. The analysis is supported by numerical simulations that cover both coded and uncoded data transmission. The complexity vs. power-efficiency trade-off of the above mentioned systems is assessed.

The paper is organized as follows: In Sec. II, the system model is introduced, and the channel model including the multiple transmit antenna extension is presented. Next, in Sec. III, different equalization strategies are discussed. For coded transmission, related decoding strategies are presented in Sec. IV. Simulation results for different scenarios and equalization strategies are provided in Sec. V. Finally, conclusions are drawn in Sec. VI.

## II. System Model

We consider a *multi-user uplink scenario* where users equipped with $N_{\mathsf{tx}}$ antennas transmit their data to a central base station equipped with $N_{\mathsf{rx}} \gg N_{\mathsf{tx}}$ antennas. An *EM lens* is placed in front of the array of receive antennas (cf. Fig. 1) [20]. The EM lens focuses the induced power on a subset of the antennas of the base station, which effectively provides multi-user spatial separation.

### A. Channel Model

We assume a uniform linear array, deployed along the $y$-axis, centered at $y = 0$. The antennas are numbered as $m = 1, \ldots, N_{\mathsf{rx}}$. The transmitter, which is placed at an angle $\vartheta_u$ against the boresight of the array, employs $N_{\mathsf{tx}}$ antennas (numbered as $l = 1, \ldots, N_{\mathsf{tx}}$ and placed also in a uniform linear array) that are sufficiently spaced such that the channels are uncorrelated. The new model in hand is an extension of the single-antenna multi-user model [20]; we define the multi-antenna transmitter by grouping several single-user transmitters into one device. We also assume that

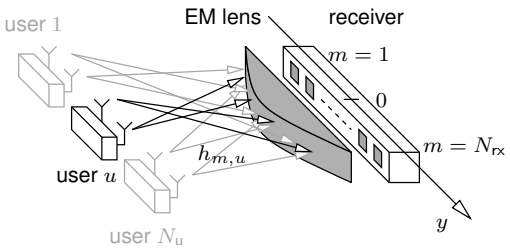


Fig. 1. Multi-user massive MIMO uplink system [13]. $N_{\mathsf{u}}$ users transmit to a central base station with $N_{\mathsf{rx}} \gg N_{\mathsf{tx}}$ antennas. An EM lens is placed in front of the base station antenna array [20]. The array model is centered at $y = 0$.

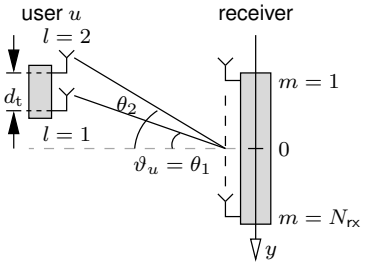


Fig. 2. Example illustrating the angle of arrival of each transmit antenna [10]. The two-antenna transmitter (with inter-antenna spacing $d_{\mathrm{t}}$) is placed in front of a linear array equipped with $N_{\mathsf{rx}}$ antennas. The angle of arrival $\theta_1$ of antenna $l = 1$ is used as the reference ($\vartheta_u$).

the EM lens provides a perfect user separation. Hence, we simplify our model to the single-user scenario.

Let $\boldsymbol{h}_l$ be the channel coefficients vector that contains the individual channel coefficients $h_{m,l}$ between transmit antenna $l$ and the base station antenna element $m$. To specify the properties of the channel, we resort to its channel covariance matrix $\boldsymbol{C}_l = \mathrm{E}\{\boldsymbol{h}_l \boldsymbol{h}_l^{\mathsf{H}}\}$.

The $f, g$ element of the covariance matrix is written as [20]

$$[\boldsymbol{C}_l]_{f,g} = \exp\left(-\frac{\sigma_\phi^2}{2}\left(\frac{2\pi d_{\mathrm{a}}}{\lambda}(f-g)\cos\theta_l\right)^2\right) \cdot \exp\left(\mathrm{j}\frac{2\pi d_{\mathrm{a}}}{\lambda}(f-g)\sin\theta_l\right) , \quad (1)$$

where $\sigma_\phi^2$ is the angular spread factor, $d_{\mathrm{a}}$ is the base station inter-antenna spacing, $\lambda$ is the wavelength of the RF carrier signal in use, and $\theta_l$ is the angle of arrival of transmit antenna $l$ [10]. The individual angles $\theta_l$ are calculated from $\vartheta_u$ as

$$\theta_l \stackrel{\text{def}}{=} \tan^{-1}\left(\tan(\vartheta_u) + (l-1)\, d_{\mathrm{t}}\right) , \quad (2)$$

where $d_{\mathrm{t}}$ is the transmitter inter-antenna spacing (cf. Fig. 2).

A construction similar to that of [20] is employed to include the effects of the EM lens on the channel model. First, the spatial position $y(\theta_l)$ of the maximum power induced for a given angle of arrival $\theta_l$ is calculated via

$$y(\theta_l) = -\frac{d_{\mathrm{a}}\,(2\Delta - N_{\mathsf{rx}} + 1)\,\theta_l}{\Theta} , \quad \theta_l \in \mathbb{R} . \quad (3)$$

Here, $\Delta$ designates the EM lens focusing parameter, which defines how many antennas the receive power is induced on (i.e., the induced power footprint), and $\Theta$ is the (total) base station coverage angle. Following this design, as long as the user antennas $l$ are within the base station coverage angle, i.e., $\theta_l \in \left[-\frac{\Theta}{2}, \frac{\Theta}{2}\right]$, the induced power is focused on the array elements and no power is lost.

Next, the position of the antenna closest to $y(\theta_l)$ is calculated via

$$\bar{m} = \frac{N_{\mathsf{rx}}}{2} + \left\lfloor \frac{y(\theta_l)}{d_{\mathrm{a}}} \right\rceil , \quad (4)$$

where $\bar{m} \in \{1, \ldots, N_{\mathsf{rx}}\}$, and $\lfloor \cdot \rceil$ denotes rounding to the next integer. Following the same argumentation as in [13], i.e., that the average receive power obeys a pure path loss model, we define the receive power distribution over the antenna elements $m$ as

$$p_m = c_{\mathsf{p}} \cdot \mathrm{e}^{-\frac{|m-\bar{m}|^2}{2\Delta^2}} , \quad (5)$$

which ensures that $95\%$ of the induced power is focused on a $4\Delta$ antenna footprint $(-2\Delta, \ldots, 2\Delta)$, centered at $\bar{m}$. The normalization constant $c_{\mathsf{p}}$ is used to ensure that the total power induced on the antenna array remains constant with and without the use of the EM lens, i.e., the EM lens is lossless and acts as a power focusing device, and power control is applied at the transmitter. The normalization constant then reads $\sum_{m=1}^{N_{\mathsf{rx}}} p_m = N_{\mathsf{rx}}$.

To include the focusing effect of the EM lens, the channel covariance matrix is finally extended to [20]

$$\bar{\boldsymbol{C}}_l = \boldsymbol{P}\boldsymbol{C}_l\boldsymbol{P} , \quad (6)$$

where $\boldsymbol{P} \stackrel{\text{def}}{=} \mathbf{diag}(\sqrt{p_m}),\ m = 1, \ldots, N_{\mathsf{rx}}$, is a diagonal matrix with entries $\sqrt{p_m}$ that denotes the spatial power distribution of the EM lens. By changing the values of the angular spread factor $\sigma_\phi^2$, the receiver-side inter-antenna distance $d_{\mathrm{a}}$, and the power distribution matrix $\boldsymbol{P}$, all scenarios ranging from a line-of-sight (LOS) channel ($\sigma_\phi^2 = 0$) to i.i.d. channels ($d_{\mathrm{a}} \gg \lambda$) and systems without an EM lens ($\boldsymbol{P} = \boldsymbol{I}$) can be modeled. The channel coefficient vectors $\boldsymbol{h}_l$ are then drawn from a zero-mean circular-symmetric complex Gaussian multivariate distribution with covariance matrix $\bar{\boldsymbol{C}}_l$, i.e., $\boldsymbol{h}_l \sim \mathcal{N}(\boldsymbol{0}, \bar{\boldsymbol{C}}_l)$.

### *B. Equivalent MIMO System Model*

Since the EM lens effectively removes the inter-user interference (by means of spatially separating the users and restricting the induced power of each user into a separate footprint), the channel model can be reduced to a single-user (point-to-point) MIMO scenario. As a consequence, the statistical channel model (6) universally describes the channel between an arbitrary user and the base station. In addition, the channel coefficients are assumed to be constant over a burst of $N_{\mathsf{bl}}$ symbols.

We assume that each user wants to transmit $N_{\mathsf{tx}}$ parallel data streams, i.e., one data stream per antenna (maximum

multiplexing gain). In the transmitter (Fig. 3), following the philosophy of bit-interleaved coded modulation (BICM) [1], [8], blocks of binary input symbols $\boldsymbol{q} \in \mathbb{F}_2^{k_\mathrm{c}}$ are encoded and randomly interleaved ($\Pi$; producing the bits $\boldsymbol{c} \in \mathbb{F}_2^{n_\mathrm{c}}$). Thereby, $R_\mathrm{c} = k_\mathrm{c}/n_\mathrm{c}$ is the code rate. Subsequently, the bits are mapped to a vector of data symbols $\boldsymbol{a} \in \mathcal{A}^{n_\mathrm{c}/\log_2(M)}$ (mapping $\mathcal{M}$), where $\mathcal{A}$ denotes a zero-mean signal constellation with cardinality $M$ and variance $\sigma_\mathsf{a}^2$. The data symbols are finally demultiplexed into $N_\mathsf{tx}$ streams, represented by the matrix of data symbols $\boldsymbol{A} = [\boldsymbol{a}_1^\mathsf{H}, \ldots, \boldsymbol{a}_{N_\mathsf{tx}}^\mathsf{H}]^\mathsf{H} \in \mathcal{A}^{N_\mathsf{tx} \times N_\mathsf{bl}}$, with the block length $N_\mathsf{bl} = n_\mathrm{c}/(N_\mathsf{tx}\log_2(M))$. Thus, the matrix $\boldsymbol{A}$ represents one binary codeword.

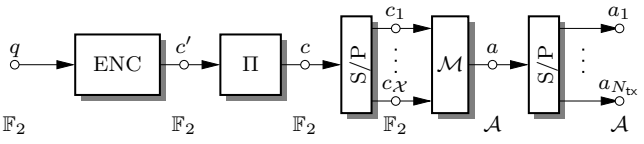


Fig. 3. System model of the transmitter [8]. The binary information symbols $\boldsymbol{q}$ are encoded into $\boldsymbol{c}'$, interleaved ($\Pi$) to produce $\boldsymbol{c}$ and are then mapped to the transmit symbols $\boldsymbol{a}$. After mapping, the transmit symbols are divided into $N_\mathsf{tx}$ parallel streams for transmission.

Before radiation, the matrix of data symbols is (jointly) preprocessed in order to obtain the matrix of transmit symbols $\boldsymbol{X} = [\boldsymbol{x}_1^\mathsf{H}, \ldots, \boldsymbol{x}_{N_\mathsf{tx}}^\mathsf{H}]^\mathsf{H} \in \mathbb{C}^{N_\mathsf{tx} \times N_\mathsf{bl}}$. The preprocessing is performed in such a way that the transmit symbols have the variance $\sigma_\mathsf{x}^2 = \sigma_\mathsf{a}^2$.

The block-based transmission is described by the MIMO system equation

$$\boldsymbol{R} = \boldsymbol{H}\boldsymbol{X} + \boldsymbol{N} \; . \tag{7}$$

Thereby, the matrix $\boldsymbol{H} = [\boldsymbol{h}_1, \ldots, \boldsymbol{h}_{N_\mathsf{tx}}] \in \mathbb{C}^{N_\mathsf{rx} \times N_\mathsf{tx}}$ consists of the channel coefficient (row) vectors $\boldsymbol{h}_l$ which are randomly chosen according to (6). Moreover, the matrix $\boldsymbol{N} \in \mathbb{C}^{N_\mathsf{rx} \times N_\mathsf{bl}}$ collects zero-mean circular-symmetric Gaussian noise samples $n_{m,k}$ with variance $\sigma_\mathsf{n}^2$. At the base station, we finally obtain our receive symbols which are combined into $\boldsymbol{R} \in \mathbb{C}^{N_\mathsf{rx} \times N_\mathsf{bl}}$.

## III. Equalization Strategies

Since $N_\mathsf{rx} \gg N_\mathsf{tx}$, joint transmitter-/receiver-side or pure receiver-side equalization schemes have to be employed in order to handle the multi-antenna interference. In contrast, conventional preequalization/precoding techniques are not suited (since, to that end, $N_\mathsf{rx} \leq N_\mathsf{tx}$ is required).

In particular, for point-to-point MIMO, the SVD is a straightforward linear joint transmitter- and receiver-side approach. More powerful is the concept of LRA LE. It is, however, a pure receiver-side technique that has—at least in the coded case—strict constraints w.r.t. channel code and signal constellation.

In the following, we first review the concepts of SVD and (conventional) LRA LE. Following this, we adapt the philosophy of LRA equalization to the point-to-point scenario, i.e., we split the channel equalization into a transmitter and a receiver part, keeping the advantages of LRA LE and avoiding its disadvantages.

### A. Singular-Value Decomposition

For the case $N_\mathsf{rx} \geq N_\mathsf{tx}$, the SVD of the MIMO channel is defined as [16]

$$\boldsymbol{H} = \boldsymbol{U}\boldsymbol{\Sigma}\boldsymbol{V}^\mathsf{H} \; , \tag{8}$$

with the unitary matrix $\boldsymbol{U} \in \mathbb{C}^{N_\mathsf{rx} \times N_\mathsf{rx}}$, the diagonal matrix $\boldsymbol{\Sigma} = \mathbf{diag}(\varsigma_1, \ldots, \varsigma_{N_\mathsf{tx}}) \in \mathbb{C}^{N_\mathsf{rx} \times N_\mathsf{tx}}$ which represents the sorted singular values $\varsigma_1 \geq \cdots \geq \varsigma_{N_\mathsf{tx}}$, and the unitary matrix $\boldsymbol{V}^\mathsf{H} \in \mathbb{C}^{N_\mathsf{tx} \times N_\mathsf{tx}}$.

The related transmission model is depicted in Fig. 4 (Top): At the joint transmitter, the matrix of data symbols is preequalized via $\boldsymbol{V}$. Since this matrix is unitary, the transmit power is kept constant, particularly we have $\sigma_\mathsf{x}^2 = \sigma_\mathsf{a}^2$. At the receiver side, the matrix of receive symbols is equalized via $\boldsymbol{\Sigma}^{-1}\boldsymbol{U}^\mathsf{H}$ before decoding.

Via this procedure, we obtain $N_\mathsf{tx}$ decoupled AWGN channels with noise variance $\tilde{\sigma}_{\mathsf{n},l}^2 = \sigma_\mathsf{n}^2/\varsigma_l^2$, $l = 1, \ldots, N_\mathsf{tx}$. Given the case that all data streams employ the same type of (coded) modulation and the same data and code rate, the transmission performance is dominated by the channel with the lowest singular value, i.e., the noise power

$$\tilde{\sigma}_{\mathsf{n},\max}^2 = \sigma_\mathsf{n}^2/\varsigma_{N_\mathsf{tx}}^2 \; . \tag{9}$$

For the conventional i.i.d. complex Gaussian channel model (i.e., uncorrelated coefficients, cf. Sec. II), it is well-known that a restriction to diversity order $D = N_\mathsf{rx} - N_\mathsf{tx} + 1$ is present.[1]

### B. Lattice-Reduction-Aided Equalization

*1) Lattice-Reduction-Aided Linear Equalization:* Conventional LRA LE [19], [18] has originally been designed for the *MIMO multiple-access channel* scenario, where several (single-antenna) users transmit their data to one joint receiver without any kind of cooperation. The related system model is depicted in Fig. 4 (Middle). Since joint transmitter-side processing is neglected, the data symbols are directly radiated. Hence, we have the (row) vectors $\boldsymbol{x}_l = \boldsymbol{a}_l$, $l = 1, \ldots, N_\mathsf{tx}$, and thus $\sigma_\mathsf{x}^2 = \sigma_\mathsf{a}^2$.

In order to perform LRA LE, the channel is factorized into

$$\boldsymbol{H} = \boldsymbol{H}_\mathrm{red}\boldsymbol{Z} \; . \tag{10}$$

More specifically, we have a *reduced* non-integer part $\boldsymbol{H}_\mathrm{red} \in \mathbb{C}^{N_\mathsf{rx} \times N_\mathsf{tx}}$ and an integer part $\boldsymbol{Z} \in \mathbb{G}^{N_\mathsf{tx} \times N_\mathsf{tx}}$, which is unimodular ($|\det(\boldsymbol{Z})| = 1$) and describes a change of basis for equalization. Thereby, $\mathbb{G} = \mathbb{Z} + \mathrm{j}\,\mathbb{Z}$ denotes the Gaussian integer lattice. Given the channel factorization (10), the equalization is performed as follows: After transmission over the MIMO channel, the matrix of noisy input symbols $\boldsymbol{R}$ is linearly equalized in a suited basis via $\boldsymbol{F} = \boldsymbol{H}_\mathrm{red}^+ = (\boldsymbol{H}_\mathrm{red}^\mathsf{H}\boldsymbol{H}_\mathrm{red})^{-1}\boldsymbol{H}_\mathrm{red}^\mathsf{H}$, i.e., the left pseudoinverse of $\boldsymbol{H}_\mathrm{red}$. After decoding, the change of basis is reversed via $\boldsymbol{Z}^{-1} \in \mathbb{G}^{N_\mathsf{tx} \times N_\mathsf{tx}}$, finally resulting in the matrix of estimated symbols $\hat{\boldsymbol{A}}$.

For the i.i.d. complex Gaussian channel model, it has been proven that this approach exploits the diversity order of the

[1] The diversity order describes the slope of the symbol/bit error curve. Given diversity order $D$, a decrease of $D$ decades in error rate is present for an increase in signal-to-noise ratio (SNR) of 10 dB.

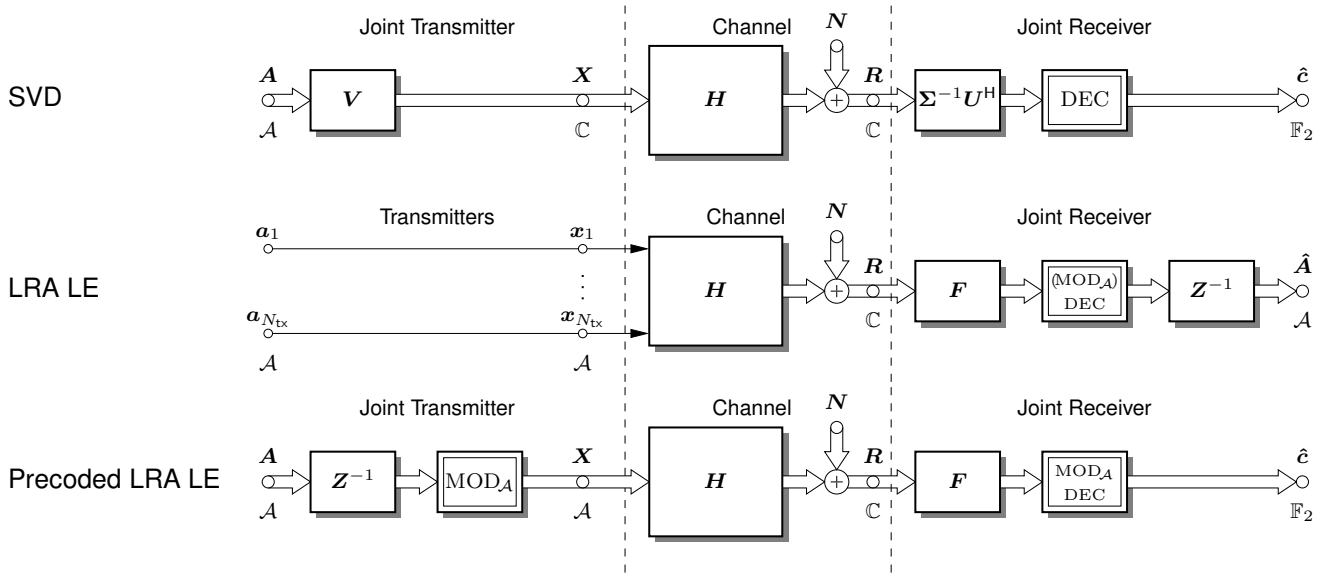


Fig. 4. Top: point-to-point MIMO transmission via SVD. Middle: conventional LRA LE for multipoint-to-point transmission. Bottom: precoded LRA LE for point-to-point transmission. In case of SVD and precoded LRA LE, a binary code and BICM is assumed.

MIMO channel, i.e., we have $D = N_{\mathsf{rx}}$ [15]. However, when applying LRA LE, a big problem is the combination with (soft-decision) channel decoding. Specifically, after non-integer equalization via $\boldsymbol{F}$, the cascade

$$\Upsilon_{\mathrm{dec}} = \boldsymbol{F}\boldsymbol{H}\boldsymbol{A} = \boldsymbol{Z}\boldsymbol{A} \tag{11}$$

is present, i.e., linear combinations of the data symbols (and hence the related codewords) have to be decoded (cf. Fig. 4). As a consequence, very strict demands on code and signal constellation are imposed: the code has to be linear, and both code and constellation have to share a joint modulo-periodic finite-field arithmetic, cf., [21], [5]. For these special constellations, a direct mapping from bits to constellation points is not possible [14]. Particularly, non-linear binary approaches like BICM cannot be applied. Hence, for the binary transmission scenario in hand, LRA LE is not a suited strategy.

*2) Precoded Lattice-Reduction-Aided Linear Equalization:* Since, in our scenario, a point-to-point transmission is present, we can take advantage of a joint preprocessing at the transmitter (cf. SVD). Hence, we are able to split the concept of LRA LE into a transmitter- and receiver-side equalization part as depicted in Fig. 4 (Bottom).

Thereby, the non-integer equalization via $\boldsymbol{F}$ has to remain at the receiver as $N_{\mathsf{rx}} \geq N_{\mathsf{tx}}$. However, the integer equalization may be moved to the transmitter since $\boldsymbol{Z}\boldsymbol{Z}^{-1} = \boldsymbol{Z}^{-1}\boldsymbol{Z} = \boldsymbol{I}$, i.e., an integer preequalization can be employed. In order to limit the transmit power, the preequalized symbols are modulo-reduced by analogy with Tomlinson-Harashima precoding or LRA precoding [18] w.r.t. a modulo-periodic signal constellation $\mathcal{A}$ (denoted as $\mathrm{MOD}_{\mathcal{A}}$). After modulo reduction, the preequalized symbols are again drawn from $\mathcal{A}$ and—since the statistical distribution of the data symbols is preserved [4]—we obtain the desired transmit power property $\sigma_{\mathsf{x}}^2 = \sigma_{\mathsf{a}}^2$. We call this strategy *precoded LRA LE*.

A convenient way to define the modulo operation in dependency of the signal constellation is to use the interaction of *signal-point lattice* $\Lambda_{\mathsf{a}}$ and *precoding lattice* $\Lambda_{\mathsf{p}}$ [6], [3], [14]. Thereby, the signal-point lattice is the lattice the data symbols are drawn from (neglecting a constant offset in order to be zero-mean). For QAM constellation we, e.g., have $\Lambda_{\mathsf{a}} = \mathbb{G}$. The precoding lattice defines the *shaping region*, i.e., the boundaries of the modulo operation and thus the related cardinality of the constellation $M$. In particular, the modulo operation is given as

$$\mathrm{MOD}_{\mathcal{A}}\{z\} = z - \mathcal{Q}_{\Lambda_{\mathsf{p}}}\{z\}\,, \tag{12}$$

where $\mathcal{Q}_{\Lambda_{\mathsf{p}}}\{\cdot\}$ denotes the quantization (Voronoi cell) w.r.t. $\Lambda_{\mathsf{p}}$. It is common practice to choose the precoding lattice as a scaled version of the signal-point lattice [14], i.e., $\Lambda_{\mathsf{p}} = \psi\Lambda_{\mathsf{a}}$, where $\psi$ is the scaling factor. $M$-ary square-QAM constellation are, e.g., obtained via $\Lambda_{\mathsf{p}} = \sqrt{M}\,\mathbb{G}$. As a consequence, the related modulo function reads

$$\begin{aligned}\mathrm{MOD}_{\mathcal{A},\mathsf{QAM}}\{z\} &= z - \mathcal{Q}_{\sqrt{M}\,\mathbb{G}}\{z\} \\ &= z - \sqrt{M}\,\mathcal{Q}_{\mathbb{G}}\left\{\frac{z}{\sqrt{M}}\right\}\,,\end{aligned} \tag{13}$$

i.e., it can be realized with a simple quantization to $\mathbb{G}$.

When applying precoded LRA LE, before decoding we obtain the cascade

$$\mathrm{MOD}_{\mathcal{A}}\{\Upsilon_{\mathrm{dec}}\} = \mathrm{MOD}_{\mathcal{A}}\left\{\boldsymbol{F}\boldsymbol{H}\,\mathrm{MOD}_{\mathcal{A}}\{\boldsymbol{Z}^{-1}\boldsymbol{A}\}\right\} = \boldsymbol{A}\,. \tag{14}$$

Thus, precoded LRA LE has the big advantage that the decoder may directly operate on (modulo-congruent) data symbols instead of their linear combinations as in case of LRA LE. As a consequence, conventional (square-)QAM constellations and non-linear coded-modulation schemes like BICM can be applied.

In order to perform precoded LRA LE according to the zero-forcing (ZF) criterion, we calculate the channel factorization (10) by applying the polynomial-time *Lenstra-Lenstra-Lovász* algorithm,[2] specifically its complex-valued variant CLLL [7]. We obtain $N_{\mathsf{tx}}$ decoupled modulo-AWGN channels with noise variance $\tilde{\sigma}^2_{\mathsf{n},l} = \sigma^2_{\mathsf{n}} \, \|\boldsymbol{f}_l^{\mathsf{H}}\|^2$, $l = 1, \ldots, N_{\mathsf{tx}}$, i.e., the (squared) row norms determine the transmission performance. In particular, when applying the same code and rate for each of the streams, the performance is dominated by the maximum noise variance

$$\tilde{\sigma}^2_{\mathsf{n},\max} = \max_{l=1,\ldots,N_{\mathsf{tx}}} \sigma^2_{\mathsf{n}} \, \|\boldsymbol{f}_l^{\mathsf{H}}\|^2 \, . \tag{15}$$

## IV. Soft-Decision Decoding

In the following, we briefly describe how to perform a soft-decision decoding when the equalization schemes from Sec. III are applied. Particularly, since binary source symbols are present, we restrict to transmission via SVD and precoded LRA LE.

In both cases, the decoding is performed according to Fig. 5. The $N_{\mathsf{tx}}$ blocks in the matrix of equalized symbols $\tilde{\boldsymbol{R}} = [\tilde{\boldsymbol{r}}_1^{\mathsf{H}}, \ldots, \tilde{\boldsymbol{r}}_{N_{\mathsf{tx}}}^{\mathsf{H}}]^{\mathsf{H}} \in \mathbb{C}^{N_{\mathsf{tx}} \times N_{\mathsf{bl}}}$ are used to calculate the log-likelihood ratios (LLRs) of the related bits (denoted as $\mathcal{L}$ and discussed below). We obtain the vectors of LLRs $\boldsymbol{\ell}_l \in \mathbb{R}^{n_{\mathrm{c}}/N_{\mathsf{tx}}}$, $l = 1, \ldots, N_{\mathsf{tx}}$. For simplicity, we write $n_{\mathsf{bl}} = n_{\mathrm{c}}/N_{\mathsf{tx}}$. These vectors are serialized to one block $\boldsymbol{\ell} \in \mathbb{R}^{n_{\mathrm{c}}}$. After deinterleaving via $\Pi^{-1}$, channel decoding is performed. It finally results in the vector of estimated bits $\hat{\boldsymbol{c}} \in \mathbb{F}_2^{k_{\mathrm{c}}}$.

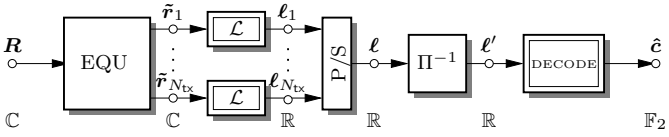


Fig. 5. System model of the receiver. After equalization (EQU), the $N_{\mathsf{tx}}$ vectors of LLRs $\boldsymbol{\ell}_l$ are calculated in dependency of the equalization scheme. They are serialized to one vector $\boldsymbol{\ell}$. After reverting the interleaving, channel decoding is performed to obtain the vector of estimated bits $\hat{\boldsymbol{c}}$.

The metric calculation depends on the actual equalization scheme. In particular, for the SVD, we have to deal with decoupled AWGN channels and in case of precoded LRA LE, decoupled modulo-AWGN channels are present.

### A. LLRs for Singular Value Decomposition

Given the case of $N_{\mathsf{tx}}$ decoupled AWGN channels with noise variance $\sigma^2_{\mathsf{n},l} = \sigma^2_{\mathsf{n}}/\varsigma_l^2$, the LLRs of the related bits $n = 1, \ldots, n_{\mathsf{bl}}$ are calculated via

$$\ell_{l,n} = \log\left( \frac{\sum_{s \in S_\nu^{(0)}} \mathrm{e}^{-|\tilde{r}_{l,\mu} - s|^2 \varsigma_l^2 / \sigma^2_{\mathsf{n}}}}{\sum_{s \in S_\nu^{(1)}} \mathrm{e}^{-|\tilde{r}_{l,\mu} - s|^2 \varsigma_l^2 / \sigma^2_{\mathsf{n}}}} \right) \, , \tag{16}$$

where $\mu = \lfloor n / \log_2(M) \rfloor + 1$ and $\nu = (n \bmod \log_2(M)) + 1$. Thereby, $S_\nu^{(0)}$ and $S_\nu^{(1)}$ denote the sets of constellation points where the bit at position $\nu = 1, \ldots, \log_2(M)$ within the $\mu^{\text{th}}$ symbol of the block is zero or one, respectively.

[2]Instead of factorizing the channel matrix directly according to (10), it is advantageous to factorize $\boldsymbol{H}^{+\mathsf{H}} = \boldsymbol{F}^{\mathsf{H}} \boldsymbol{Z}^{-\mathsf{H}}$, i.e., the Hermitian of the pseudo-inverse of $\boldsymbol{H}$. Then, the reduction criteria directly operate on the non-integer equalization matrix $\boldsymbol{F}$, which may improve the transmission performance. This is known as dual-lattice approach, cf. [15], [5].

### B. LLRs for Precoded Lattice-Reduction-Aided Linear Equalization

For the case of $N_{\mathsf{tx}}$ decoupled modulo-AWGN channels with noise variance $\sigma^2_{\mathsf{n},l} = \sigma^2_{\mathsf{n}} \|\boldsymbol{f}_l^{\mathsf{H}}\|^2$, the situation is more complicated. Specifically, due to the transmitter-side modulo operation, an infinite number of modulo-congruent constellation points has to be incorporated when calculating the optimal soft information. Since this is not possible in practice, approximative approaches have to be applied. In the mid-to-high SNR regime, the *nearest-neighbor approximation* [3] is very close to the optimal performance, i.e., only the closest modulo-congruent point is considered. Incorporating the nearest-neighbor approximation and the adapted noise variance into (16), we obtain

$$\ell_{l,n} = \log\left( \frac{\sum_{s \in S_\nu^{(0)}} \min_{\lambda \in \Lambda_{\mathsf{p}}} \mathrm{e}^{-|\tilde{r}_{l,\mu} - s + \lambda|^2 / (\sigma^2_{\mathsf{n}} \|\boldsymbol{f}_l^{\mathsf{H}}\|^2)}}{\sum_{s \in S_\nu^{(1)}} \min_{\lambda \in \Lambda_{\mathsf{p}}} \mathrm{e}^{-|\tilde{r}_{l,\mu} - s + \lambda|^2 / (\sigma^2_{\mathsf{n}} \|\boldsymbol{f}_l^{\mathsf{H}}\|^2)}} \right) \, . \tag{17}$$

Then, the precoding lattice $\Lambda_{\mathsf{p}}$ describes all points were the periodic repetitions of the signal constellation are centered. If square-QAM constellations are employed, $\Lambda_{\mathsf{p}} = \sqrt{M}\,\mathbb{G}$ represents the periodic repetitions (cf. Sec. III).

## V. Numerical Simulations

Numerical simulations were conducted for an $N_{\mathsf{rx}} = 100$ uniform linear antenna array at the base station, employing omni-directional antenna elements. The base station coverage angle is $\Theta = \frac{2}{3}\pi$, i.e., the array can see users having an angle of arrival $\vartheta \in \left[-\frac{\pi}{3}, \, \frac{\pi}{3}\right]$. The focusing parameter $\Delta = 5$ is chosen. The SNR is represented via

$$\frac{E_{\mathsf{b}}}{N_0} = \frac{\sigma^2_{\mathsf{x}}}{\sigma^2_{\mathsf{n}} \log_2(M) R_{\mathrm{c}}} \, , \tag{18}$$

where $E_{\mathsf{b}}$ is the average energy per transmitted information bit and $N_0$ the (two-sided in ECB domain) noise-power spectral density.

The user device is equipped with $N_{\mathsf{tx}} = 4$ antennas, with an inter-antenna spacing $d_{\mathrm{t}} = \lambda$. It is placed at an angle $\vartheta = -0.48\Theta$. A 16-QAM alphabet is used for transmission. In case of coded transmission, the rate $R_{\mathrm{c}} = 1/2$ LDPC code (dimension $k_{\mathrm{c}} = 32400$, length $n_{\mathrm{c}} = 64800$) from the DVB-S2 standard [2] is employed. This results in a block length of $N_{\mathsf{bl,coded}} = 4050$ symbols. In case of uncoded transmission, a block length of $N_{\mathsf{bl,uncoded}} = 2025$ symbols is used. Belief-propagation decoding is applied with a maximum number of 50 iterations per block.

The channel remains constant for each burst of transmit symbols, and perfect channel knowledge is assumed at the receiver. The same channel coefficients are used for the coded and uncoded case. An angular spread factor $\sigma^2_\phi = 0.14$ was chosen, which corresponds to an angular spread of $5°$. The value was chosen as such according to measurement data from [10].

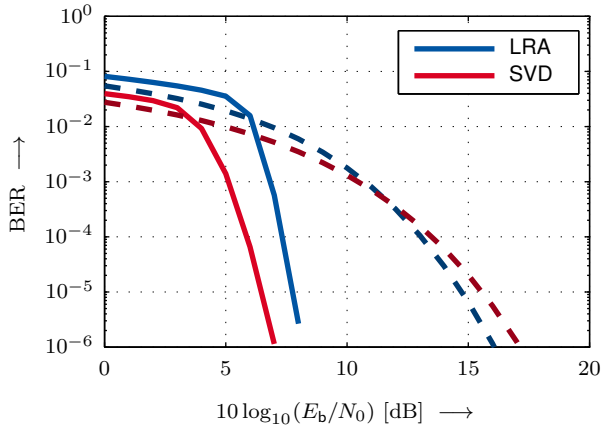


Fig. 6. Bit-error rate performance vs. SNR for the point-to-point MIMO scenario. $\sigma_\phi^2 = 0.14$. I.i.d. channel model with inter-antenna spacing $d_a = 100\lambda$. Focusing parameter $\Delta = 5$. Precoded LRA LE (blue) vs. SVD (red). Solid: coded; dashed: uncoded.

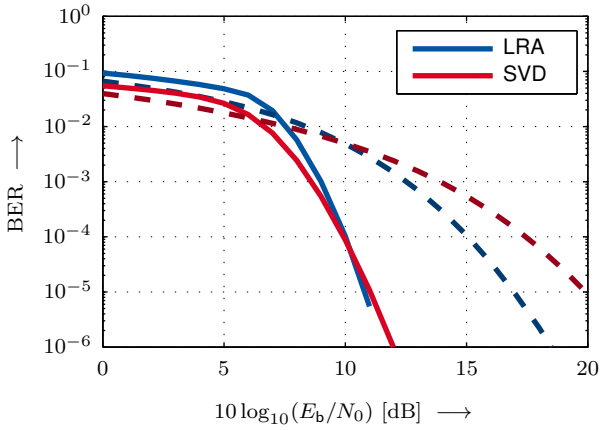


Fig. 8. Bit-error rate performance vs. SNR for the point-to-point MIMO scenario. $\sigma_\phi^2 = 0.52$. Spatially correlated channel model with inter-antenna spacing $d_a = \lambda/2$. Focusing parameter $\Delta = 5$. Precoded LRA LE (blue) vs. SVD (red). Solid: coded; dashed: uncoded.

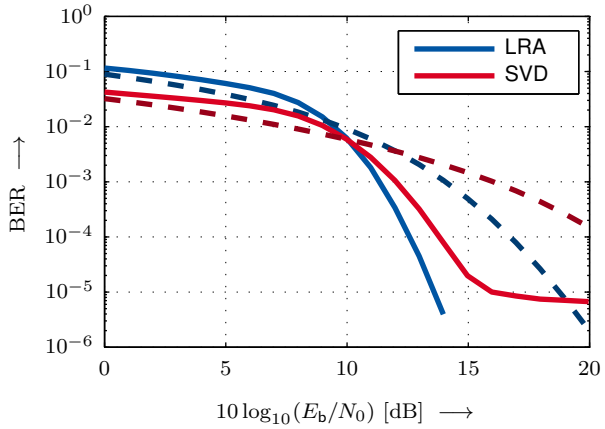


Fig. 7. Bit-error rate performance vs. SNR for the point-to-point MIMO scenario. $\sigma_\phi^2 = 0.14$. Spatially correlated channel model with inter-antenna spacing $d_a = 2\lambda$. Focusing parameter $\Delta = 5$. Precoded LRA LE (blue) vs. SVD (red). Solid: coded; dashed: uncoded.

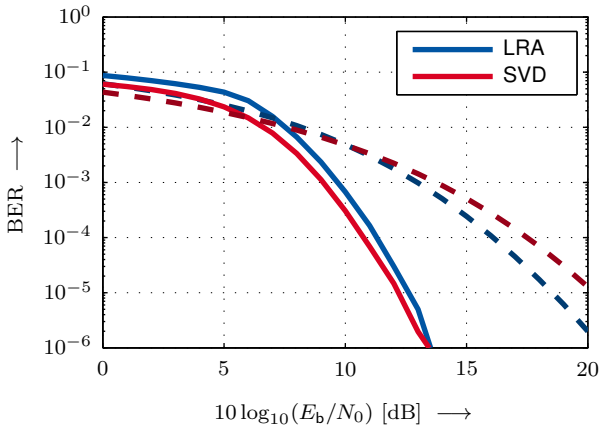


Fig. 9. Bit-error rate performance vs. SNR for the point-to-point MIMO scenario. $\sigma_\phi^2 = 0.14$. Spatially correlated channel model with inter-antenna spacing $d_a = \lambda/2$. Focusing parameter $\Delta = 5$. User positioned at $\vartheta = 0$. Precoded LRA LE (blue) vs. SVD (red). Solid: coded; dashed: uncoded.

First, we set the base station inter-antenna distance $d_a = 100\lambda$, which results in an i.i.d. channel scenario, and measure the bit-error rate of the precoded LRA system vs. the system employing the SVD. The numerical results are plotted in Fig. 6. In case of uncoded transmission, we see that the LRA system with precoding (blue, dashed) shows a gain in the higher SNR regime, since precoding achieves maximum diversity and linear precoding does not.

On the other hand, in case of coded transmission, the SVD shows a gain of approximately 1 dB at BER $= 10^{-5}$ when compared to the LRA case. This is a direct result of the LLR calculation method used for soft-input decoding. In case of the SVD, the log-likelihood ratios are calculated optimally by comparing Euclidean distances, while in case of precoding, modulo distances are required resulting in a performance loss.

Although the i.i.d. channel model is usually used as a performance baseline, for this scenario it is not realistic. This is due to the fact that, to ensure spatially decoupled channels, this results in a physically very large and unfeasible system. This is also true even when using carrier frequencies in the order of GHz (taking into account the spread factor $\sigma_\phi^2 = 0.14$). Therefore, a compromise must be made to ensure that the system can be implemented.

To achieve this, the inter-antenna spacing at the base station must be reduced. In our case, we choose a spacing of $d_a = 2\lambda$, which results in spatially correlated channels to be seen at the receiver. Again both the precoded system and the one employing the SVD are compared and the results are plotted in Fig. 7. This time, we see that in case of uncoded transmission, the system employing precoding has a significant gain over the one using the SVD. Moreover, in case of coded transmission, the SVD cannot cope with the correlated channels, which leads to a performance loss larger than the one incurred by the nonoptimal LLR calculation used in the case of precoding, and

even an error floor is exhibited. We now see that the increased complexity required for LRA precoding overcomes the losses from the channel.

Next, in Fig. 8, we simulate a system using $d_{\mathrm{a}} = \lambda/2$ spaced antenna elements under typical urban environment conditions, i.e., a scenario with a high spread factor of $\sigma_\phi^2 = 0.52$. On the one hand, we see that in the uncoded case, the LRA precoding scheme still shows a significant gain over the SVD scheme. On the other hand, in case of coded transmission, both LRA precoding and SVD show similar performance. One could argue that when employing a coded transmission system, the reduced complexity of the SVD is favorable. However, this would only apply when the channel conditions are good. If the channel gets worse, a performance similar to that of Fig. 7 is expected.

Finally, in Fig. 9, the simulation results when the user is positioned at $\vartheta = 0$ (i.e., in the antenna array boresight) are plotted. In this scenario the antennas are closely spaced ($d_{\mathrm{a}} = \lambda/2$) and the spreading factor is chosen as $\sigma_\phi^2 = 0.14$. We see in the uncoded system that the performance lies between that of the i.i.d. case and the correlated channels case, while in the coded case, there is a marginal difference in performance between LRA precoding and SVD. When placed at boresight, according to the channel model definition (cf. (1)), the first antenna experiences an i.i.d. channel, and the others weakly correlated channels (as the angle deviates less from boresight, the number of off-diagonal entries in the channel covariance matrix $\boldsymbol{C}_l$ becomes smaller, and hence the channel correlation is reduced). This again supports our previous statement; even in the best-case scenario, the higher complexity of LRA precoding would still be justifiable.

## VI. Conclusions

In this paper, we have presented an extension to the EM-lens-enabled (massive) MIMO uplink system, by increasing the number of transmitter-side antennas. With such extension, equalization strategies that are suited for classical (non-massive) MIMO are enabled. We have shown that lower-complexity equalization strategies (such as equalization via the SVD) result in significant losses in the case of spatially correlated channels. By employing precoded LRA equalization, the diversity of the MIMO channel is exploited which, especially in the case of correlated channels, offers a large increase in power efficiency. We have also shown that, although the LLR calculation on the modulo-AWGN channel is not optimal for LDPC codes in the i.i.d. case, BICM with precoded LRA LE suffers from lower losses compared to the SVD case when the channels are spatially correlated.

## References


[1] G. Caire, G. Taricco, E. Biglieri. Bit-Interleaved Coded Modulation. *IEEE Transactions on Information Theory*, pp. 927–946, May 1998.

[2] European Telecommunications Standards Institute. DVB-S2. *ETSI Standard EN 302 307 V1.1.1: Digital Video Broadcasting (DVB)*, 2005.

[3] R.F.H. Fischer. *Precoding and Signal Shaping for Digital Transmission*. Wiley-IEEE Press, 2002.

[4] R.F.H. Fischer. Lattice-Reduction-Aided Equalization and Generalized Partial-Response Signaling for Point-to-Point Transmission over Flat-Fading MIMO Channels. In *4th International Symposium on Turbo Codes and Related Topics in connection with 6th International Conference on Source and Channel Coding*, Apr. 2006.

[5] R.F.H. Fischer, M. Cyran, S. Stern. Factorization Approaches in Lattice-Reduction-Aided and Integer-Forcing Equalization. In *International Zurich Seminar on Communications*, pp. 108–112, Mar. 2016.

[6] D. Forney. Multidimensional Constellations-Part II: Voronoi Constellations. *IEEE Journal on Selected Areas in Communications*, pp. 941–958, Aug. 1989.

[7] Y.H. Gan, C. Ling, W.H. Mow. Complex Lattice Reduction Algorithm for Low-Complexity Full-Diversity MIMO Detection. *IEEE Transactions on Signal Processing*, pp. 2701–2710, July 2009.

[8] B.M. Hochwald, S. ten Brink. Achieving Near-Capacity on a Multiple-Antenna Channel. *IEEE Transactions on Communications*, pp. 389–399, Apr. 2003.

[9] T.L. Marzetta. Noncooperative Cellular Wireless with Unlimited Numbers of Base Station Antennas. *IEEE Transactions on Wireless Communications*, pp. 3590–3600, Nov. 2010.

[10] B. Ottersten. Array Processing for Wireless Communications. In *8th Workshop on Statistical Signal and Array Processing*, June 1996.

[11] F. Rusek, D. Persson, B.K. Lau, E.G. Larsson, T.L. Marzetta, O. Edfors, F. Tufvesson. Scaling Up MIMO: Opportunities and Challenges with Very Large Arrays. *IEEE Signal Processing Magazine*, 40–60, Jan. 2013.

[12] A. Schenk. *Coding, Modulation, and Detection in Impulse-Radio Ultra-Wideband Communications*, PhD Thesis. University Erlangen-Nürnberg, 2012.

[13] A. Schenk, R.F.H. Fischer. Noncoherent Detection in Massive MIMO Systems. In *International ITG/IEEE Workshop on Smart Antennas*, Mar. 2013.

[14] S. Stern, R.F.H. Fischer. Lattice-Reduction-Aided Preequalization over Algebraic Signal Constellations. In *International Conference on Signal Processing and Communication Systems*, Dec. 2015.

[15] M. Taherzadeh, A. Mobasher, A.K. Khandani. LLL Reduction Achieves the Receive Diversity in MIMO Decoding. *IEEE Transactions on Information Theory*, pp. 4801–4805, Dec. 2007.

[16] D. Tse, P. Viswanath. *Fundamentals of Wireless Communication*. Cambridge University Press, 2005.

[17] A.M. Tulino, A. Lozano, S. Verdú. Impact of Antenna Correlation on the Capacity of Multiantenna Channels, *IEEE Transactions on Information Theory*, pp. 2491–2509, July 2005.

[18] C. Windpassinger, R.F.H. Fischer. Low-Complexity Near-Maximum-Likelihood Detection and Precoding for MIMO Systems using Lattice Reduction. In *IEEE Information Theory Workshop*, pp. 345–348, Mar. 2003.

[19] H. Yao, G.W. Wornell. Lattice-Reduction-Aided Detectors for MIMO Communication Systems. In *IEEE Global Telecommunications Conference*, Nov. 2002.

[20] Y. Zeng, R. Zhang, Z.N. Chen. Electromagnetic Lens-Focusing Antenna Enabled Massive MIMO: Performance Improvement and Cost Reduction. *IEEE Journal on Selected Areas in Communications*, pp. 1194–1206, Jun. 2014.

[21] J. Zhan, B. Nazer, U. Erez, M. Gastpar. Integer-Forcing Linear Receivers. *IEEE Transaction on Information Theory*, pp. 7661–7685, Dec. 2014.